Science of Sintering, **50** (2018) 123-132

doi: https://doi.org/10.2298/SOS1801123P

UDK 546.824; 622.785

The Effect of Sintering Temperature on Mesoporous Structure of WO_3 Doped Tio_2 Powders

Srđan Petrović[1*)], Ljiljana Rožić[1], Stevan Stojadinović[2], Boško Grbić[1], Rastko Vasilić[2], Zorica Vuković[1] and Nenad Radić[1]

[1]University of Belgrade, IChTM-Department of Catalysis and Chemical Engineering, Njegoševa 12, Belgrade, Republic of Serbia

[2]University of Belgrade, Faculty of Physics, Studentski trg 12-16, 11000 Belgrade, Serbia

Abstract:

In this study, WO_3 doped TiO_2 powders were synthesized via sol-gel method combined with a hydrothermal process. The effect of sintering temperature on mesoporous structure and catalytic activities of these powders were investigated. The physical analysis via X-ray diffraction indicates that prepared samples are a mixture of anatase and rutile TiO_2 phases. X-ray peak analysis is used to evaluate the crystallite size and lattice strain by the Williamson-Hall analysis. Considering all the reflections of the anatase phase the lattice strain ranging from c = 9.505 to c = 9.548 is calculated, suggesting that microstrain decreases when calcination temperature increases. N_2 adsorption-desorption analysis shows that the surface area and pore volume decrease with increasing temperature and that WO_x-TiO_2 powders primarily consist of mesopores. Sintering temperature induced a change in textural properties causing a systematic shift towards larger mesopores. Simultaneously, photoactivity in decolorization of methyl orange increases with increasing calcination temperature up to 700 °C, followed by significant decrease with its further increase.

Keywords: *WO_x-TiO_2 powders; Sintering; Mesoporous structure; Photocatalytic degradation; Azo dye.*

1. Introduction

TiO_2 is an excellent material for environmental applications, including photodegradation of various pollutants and purification of water and air [1-3]. Conventional photocatalytic processes for organic decomposition in waste waters use TiO_2 powder as photocatalyst. Finely dispersed TiO_2 particles are usually suspended in wastewater and placed under UV irradiation [4, 5]. When TiO_2 is illuminated by UV light, electrons and holes are photogenerated within, thus oxidizing the organic compounds dissolved in water. To increase the overall efficiency of this process it is very important to develop methods for broadening the spectrum of absorbed light in the visible range and increase the photocatalytic properties of TiO_2 in both UV and visible range [6].

To improve the photocatalytic efficiency of such materials many efforts have been made, including various synthesis pathways and subsequent modification of TiO_2 powder properties. Coupling TiO_2 with other semiconducting materials is considered beneficial because coupling two semiconductors with different redox energy levels can increase the

*) **Corresponding author:** srlepp@nanosys.ihtm.bg.ac.rs

separation of their corresponding conduction and valence bands [7]. So far, the most successful results have been achieved through the loading of metal or metal oxides on the surface of TiO_2 [8-10]. Generally, metal oxides such as WO_3 and MoO_3 proved as excellent candidates for coupling with TiO_2, due to increased photocatalytic activity of [11, 12].

The structural and microstructural, morphological and photocatalytic properties of TiO_2 nanocrystals are strongly dependent on the synthesis process [13] and calcination temperature [14, 15].

Sol-gel processing has become one of the most successful techniques for preparation of TiO_2 powders and gels [16, 17]. Nevertheless, TiO_2 materials obtained by sol-gel processing are either amorphous or not well crystallized and consequently, they must undergo a suiTab. treatment to become active photocatalysts. In order to control crystallinity of TiO_2 thermal treatment is usually applied but the temperature must be carefully selected.

The temperature of anatase to rutile phase transition is around 600 °C, depending on different factors such as defects, impurities and grain size. The relationship between the microstructure and elastic properties of the rutile phase has been widely discussed [18-20], while only a few studies have been conducted for the anatase phase [21].

X-ray powder diffraction (XRD) analysis is a simple and powerful tool to estimate the crystallite size and lattice strain. This is achieved by Williamson-Hall analysis that is a simplified method where the size and strain broadening are deconvoluted by considering the peak width as a function of 2θ [22]. These analyses are employed for estimating crystallite size and lattice strain in the present study. When microstrain is neglected, the coherently diffracted domain size can simply be evaluated by the Debye - Scherrer equation [23].

In this study, WO_x-TiO_2 powders were prepared by sol-gel method combined with a hydrothermal treatment. WO_x-TiO_2 powders with varying amount of anatase and rutile phases are obtained by carefully controlling the sintering temperature. By combining two analytical techniques (XRD and N_2 adsorption-desorption), we determined the correlation between the change of phase composition, nanoparticle growth, and textural properties with sintering temperature. The strain associated with calcination of WO_x-TiO_2 samples at 500, 600, 650, 700, 750 and 800 °C due to lattice deformation was estimated by a modified form of Williamson-Hall model. In order to estimate the photocatalytic activity of WO_x-TiO_2 powders, methyl orange was employed in the photocatalytic tests.

2. Experimental

2.1. WO_x-TiO_2 powders synthesis

Titanium (IV) isopropoxide and tungstophosphoric acid were used for the synthesis of WO_x-TiO_2 powders in this study. All chemicals were of analytical grade. Amorphous powders were prepared by a sol-gel method. For the synthesis of samples, titanium isopropoxide was slowly dissolved in isopropyl alcohol. After that, an appropriate amount of $H_3PW_{12}O_{40}$ (20 %) was dissolved in water and then added into solution drop by drop. The resulting mixture was heated to 45 °C until homogeneous hydrogel was formed. This hydrogel was subsequently heated to 200 °C at a heating rate of 2 °C/min and after that washed with hot water three times. The wet gel was annealed at 500, 600, 650, 700, 750 and 800 °C for 3 hours, which resulted in the formation of WO_x-TiO_2 powders.

2.2. WO_x-TiO_2 powders characterization

The phase structure of samples was analyzed by X-ray diffraction method, using a Rigaku Ultima IV diffractometer in Bragg-Brentano geometry, with Ni-filtered CuK_α

radiation (40 kV, 30 mA, λ=1.54178 Å). The structural and microstructural parameters of TiO_2 samples were estimated by Williamson-Hall (WH) plots [22].

N_2 adsorption-desorption isotherms of all samples were measured with an automatic adsorption apparatus (Sorptomatic 1990 Thermo Finnigan) at 77 K. The specific surface areas (S_{BET}) were calculated by fitting the adsorption data to Brunauer–Emmett–Teller (BET) equation [24] and the pore size distributions were calculated by the Barrett-Joyner-Halenda method [25].

2.3. Photocatalytic tests

Photocatalytic degradation of methyl orange (MO) was carried out in an open cylindrical thermostated Pyrex cell of 6.8 cm in diameter, corresponding to the surface area accessible to the light of 36.3 cm^2. The experiments were performed with 100 mL solution containing 8 mg/L MO and 100 mg of WO_x-TiO_2 or pure TiO_2 powders. Irradiation of the solutions was performed under the lamp that simulates solar radiation (Solimed BH Quarzlampen), with a power consumption of 300 W, housed 25 cm above the top surface of the solution. Illumination intensity on the top of the photocatalytic reactor was 850 lx. Prior to illumination, the suspensions were magnetically stirred in the dark for 30 min to achieve adsorption–desorption equilibrium. Aliquots of suspensions were collected at different time intervals for a total of 150 min. The aliquots were filtered through a 0.20 μm syringe membrane filter into standard quartz cuvettes with an optical path of 1 cm and directed to UV-Vis spectrometer (Thermo Electron Nicolet Evolution 500) to check the degradation of MO via its absorption peak at 464 nm. These absorption data were used in the determination of degradation of MO through comparison with the absorbance at a certain time as a percentage of the initial absorbance.

3. Results and discussion

Physical properties of WO_x-TiO_2 powders often vary with preparation history and post-treatment. Therefore, as a first step, it is necessary to determine the structure of prepared samples.

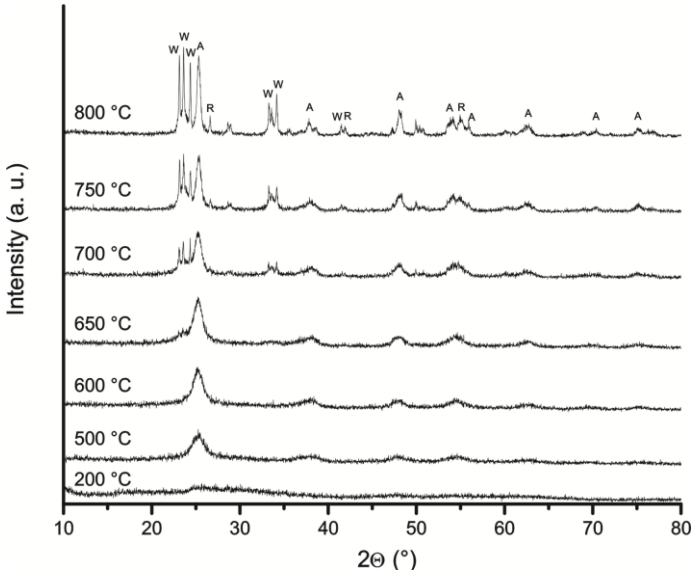

Fig. 1. XRD patterns of WO_x-TiO_2 powders for different sintering temperatures (A: anatase, R: rutile, W: tungsten oxide).

XRD patterns of prepared WO_x-TiO_2 powders (Fig. 1) without annealing feature weak broad peaks in the positions corresponding to characteristic peaks of the anatase phase. This is an indication of poorly crystallized and/or mostly amorphous solids. After annealing from 500 to 800 °C all diffraction peaks become more intense, which is related to crystallization and particle growth. However, when the annealing temperature was elevated to 700 °C, small rutile peaks are observed, indicating the onset of anatase-to-rutile transformation. In previously published papers, the beginning of the transformation of anatase-to-rutile was observed in the range 400-1200 °C [26, 27], depending on the utilization of different raw materials, processing methods and methods for determination of the transition temperature.

It was also observed that when annealing temperature goes above 600 °C, the Keggin molecule breaks up to form WO_3 species. The orthorhombic WO_3 and a non-stoichiometric form of tungsten oxide ($WO_{2.92}$) were observed in the samples annealed at 700 and 800 °C. The variation of anatase-to-rutile ratio of WO_x-TiO_2 powders are correlated with annealing temperature and presented in Tab. I. Anatase (101) peak at $2\theta = 25.48°$ and rutile (110) peak at $2\theta = 27.58°$ were analyzed using the equation [28]:

$$X = \left(1 + 0.8\frac{I_A}{I_R}\right)^{-1} \quad (1)$$

where X is the weight fraction of rutile, and I_A and I_R are the X-ray intensities of anatase and rutile peaks, respectively.

As can be seen, the anatase content estimated from equation 1 decreases from 100 to 82 % with increasing sintering temperature up to 800 °C. Also, results indicate that at 700, 750 and 800 °C all WO_x-TiO_2 samples contain much lower fraction of rutile than pure TiO_2 exposed to the same temperature treatment, which is usually transformed to rutile phase by over 90 % [26]. Obviously, WO_3 hindered the phase transformation from anatase to rutile during sintering. Annealing at elevated temperatures can induce the sintering of crystals, resulting in an increase in the crystallite size. Gaining enough energy could position the crystallite in proper equilibrium sites resulting in improved crystallinity and degree of orientation [29].

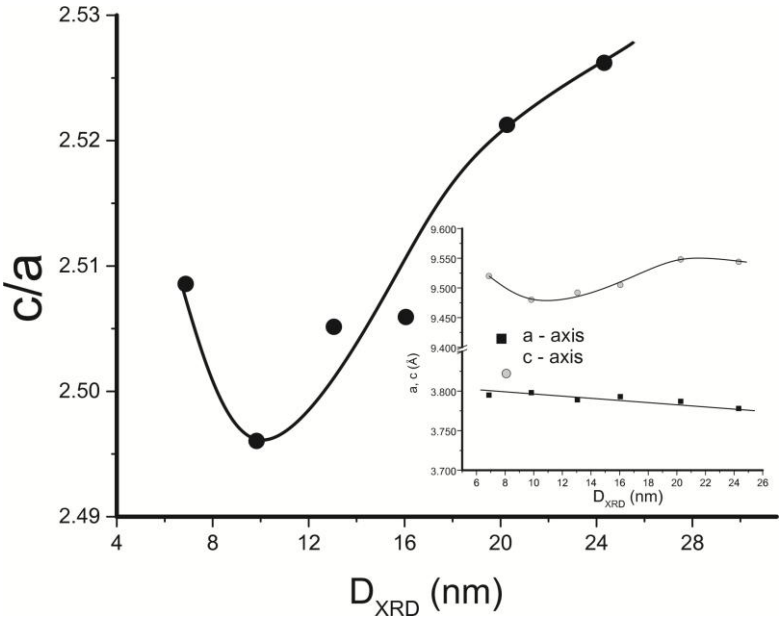

Fig. 2. Dependence of the '*c/a*' ratio for the anatase phase of WO_x-TiO_2 samples. The insert shows the corresponding variation of '*a*' and '*c*' lattice parameters.

The value of lattice parameters $a = b$ and c of anatase phase in samples calcined at various temperatures as a function of the growth of crystallites are shown at Fig. 2. The continuous increase of the unit cell ratio (c/a) occurs with increasing calcination temperature and concurrent crystallite growth, mainly originates from stretching in the direction of the c-axis and, to a lesser extent, in the small shortening of a-axis (insert of Fig. 2). This particular value of c-axis together with a relatively weak variation of a-axis has been identified for nanocrystalline TiO_2 [30].

XRD pattern can be utilized to evaluate the narrowing of peaks with the growth of the crystallites and lattice strain. If strain contribution is neglected, the particle size can be estimated from the Scherrer equation, while better estimation of size and strain can be made from WH method. Williamson and Hall proposed a method for deconvolution of size and strain broadening based on the peak width as the function of 2 θ. If a linear fit is obtained from the equation:

$$\beta_{hkl} = \frac{K\lambda}{D\cos\theta} + 4\varepsilon\sin\theta \quad (2)$$

it is possible to derive the crystallite size (D_{XRD}) from the intercept, and micro-strain (ε) from the slope. K is a constant equal to 0.94 for spherically shaped particles, λ is the wavelength of the x-ray (1.54178 Å for CuK_α radiation) and θ is the peak center. Figure 3(a)-(f) represents the W-H plot of annealed WO_x-TiO_2 samples. The experimental data points are shown with symbols and fitted data points are shown with the straight line. As can be seen from Fig. 3, the microstrain gradually increases with increasing calcination temperature up to 700 °C and then decreases at higher temperatures. On the other hand, the particle size progressively increases with increasing calcination temperature (Tab. I).

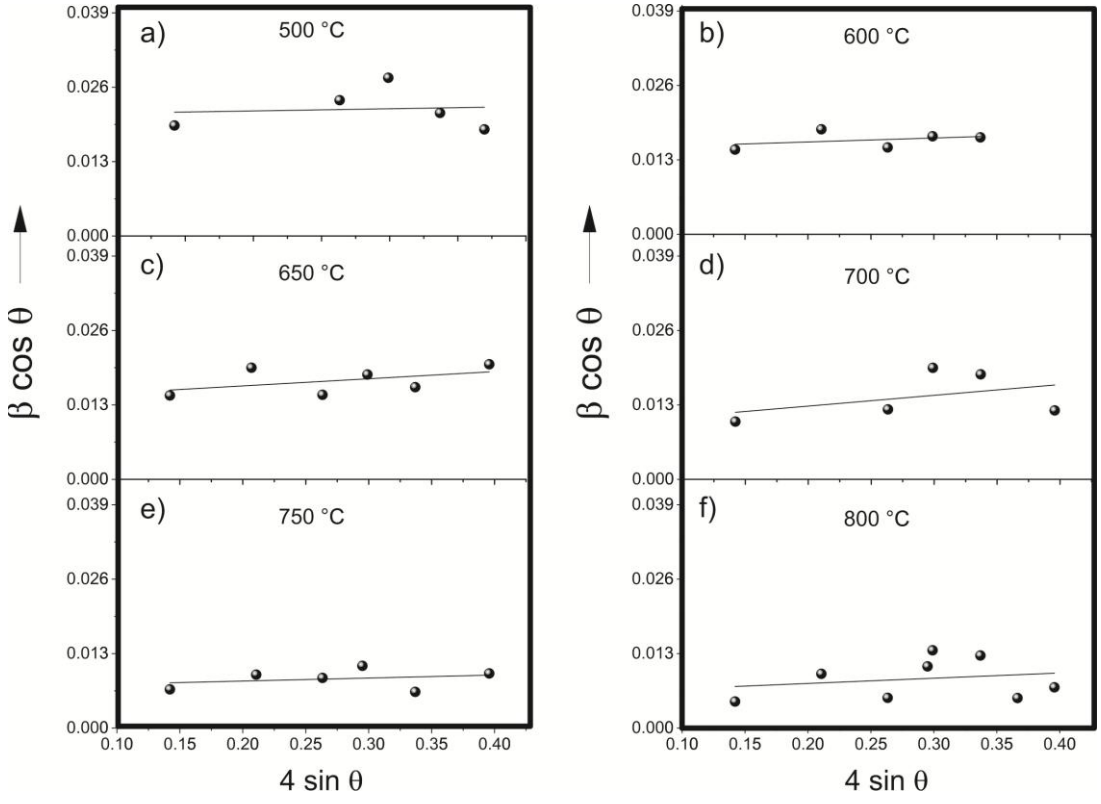

Fig. 3. Williamson-Hall plot for WO_x-TiO_2 samples obtained for different calcination temperatures.

Tab. I Phase composition and average crystallite size of anatase obtained by Williamson-Hall method.

Sample	Weight fraction of Anatase (%)	Weight fraction of Rutile (%)	W-H method D (nm)
WO_x-TiO_2 (500)	100	-	6.87
WO_x-TiO_2 (600)	100	-	9.83
WO_x-TiO_2 (650)	-	-	13.05
WO_x-TiO_2 (700)	88.49	11.51	16.05
WO_x-TiO_2 (750)	85.31	14.69	20.27
WO_x-TiO_2 (800)	82.04	17.96	24.32

Dynamics of all these changes should be considered through mechanism of the process. It should be kept in mind that above 650 °C simultaneously three processes occur; sintering, anatase-to-rutile phase transformation, and decomposition of Keggin anion to WO_x species.

Pore size distribution, BET surface area, and pore volume were obtained by N_2 adsorption analysis (Tab. II). BET surface area and pore volume of WO_x-TiO_2 samples decreases as the calcination temperature increases, which is in accordance with sintering process. It has been reported [31] that the main contribution to the surface area comes from small pores, while macropores have smaller contribution. Smaller pores have narrow, while larger pores have broader pore size distribution. Obviously, small micropores (3.7 nm) did not change while the larger ones continuously increased from 8.8 to 21 nm, upon thermal treatment (Tab. II). Besides, with raising the sintering temperature, the relative amount of smaller sized mesopores decreased gradually and disappears at 800 °C, while the relative amount of the larger ones constantly increases.

Tab. II Textural properties of WO_x-TiO_2 powders after calcination at different temperatures.

Sample	S_{BET} (m^2g^{-1})	V_{tot} (cm^3g^{-1})	V_{mic} (cm^3g^{-1})	d_{max1} (nm)	d_{max2} (nm)
WO_x-TiO_2 (500)	130.8	0.301	0.046	3.74	7.99
WO_x-TiO_2 (600)	101.4	0.278	0.035	3.67	9.54
WO_x-TiO_2 (650)	78.7	0.256	0.027	3.61	10.49
WO_x-TiO_2 (700)	67.4	0.260	0.023	3.62	11.24
WO_x-TiO_2 (750)	52.2	0.239	0.017	3.60	12.81
WO_x-TiO_2 (800)	35.3	0.215	0.012	3.70	20.55

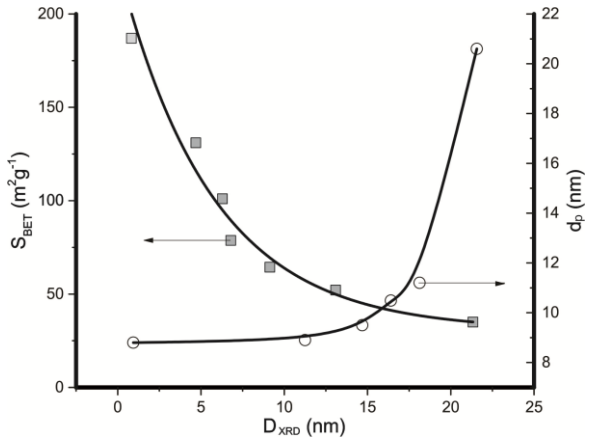

Fig. 4. Crystal size (D_{XRD}), pore size (d_p) and specific surface area (S_{BET}) for WO_x-TiO_2 powders sintered at different temperatures (from 500 to 800 °C).

Comparison of microstructural properties (specific surface area - S_{BET} and pore size- d_{BET}) and crystallite size - D_{XRD} as a function of thermal treatment is represented in Fig. 4. With increasing sintering temperature the average crystallite size of anatase increases, while specific surface area of WO_x-TiO_2 decreases. Also, WO_x-TiO_2 samples (calcined from 500 to 700 °C) have similar total pore volume and average pore size at corresponding crystallite size. These observations indicate that samples undergo similar particle growth and aggregation during the thermal treatment.

Considering that calcination temperature is an important parameter that affects the structure and photocatalytic activity of TiO_2 [31], WO_x-TiO_2 samples prepared at different calcination temperatures were tested for photocatalytic degradation of MO under visible-light illumination. Also, in order to compare the degree of decomposition of MO over WO_x-TiO_2 samples we presented results for pure TiO_2 calcinated at 500 ^oC (Fig. 5a). TiO_2 (500) sample showed higher photocatalytic activity towards MO degradation than TiO_2 samples calcinated at high temperatures, 600, 650, 700, 750, and 800 ^oC. For this reason, TiO_2 (500) sample was selected as a reference material.

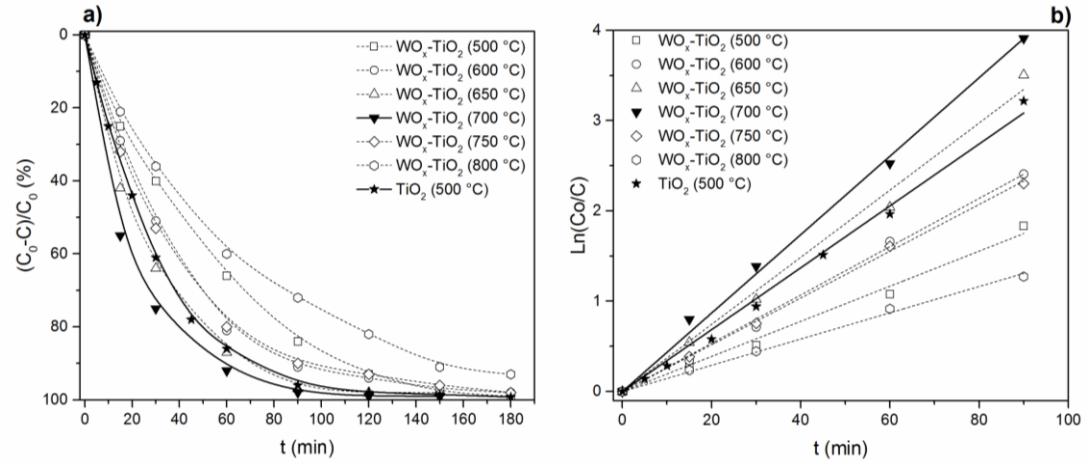

Fig. 5. Degradation rate of MO (%) over WO_x-TiO_2 powders and TiO_2 (500) versus time interval (a) and first-order kinetic plot (b).

Observed photodegradation rate of MO over pure TiO_2 and WO_x-TiO_2 samples show that increasing calcination temperature from 500 to 700 °C leads to an increase of photocatalytic activity. Further increase of the calcination temperature to 800 °C leads to significant reduction of *BET* surface area and pore volume (Tab. II), resulting in noTab. drop of MO degradation rate. It is also observed that an increase of irradiation time rapidly decreases the concentration of MO, suggesting fast photodegradation of MO on the surface of WO_x-TiO_2 powders.

The kinetic data fit well to the Langmuir Hinshelwood model:

$$\ln\left(\frac{C_0}{C}\right) = kt \tag{4}$$

where k is apparent reaction constant rate (min^{-1}), C_0 and C are initial and reaction concentration of MO, respectively and t is time of irradiation. Kinetic data are displayed in Fig. 5b and Tab. III.

Tab. III Rate constants of TiO_2 (500) and WOx-TiO_2 photocatalysts calcined at different temperature.

Sample	TiO_2 (500)	WO_x-TiO_2 (500)	WO_x-TiO_2 (600)	WO_x-TiO_2 (650)	WO_x-TiO_2 (700)	WO_x-TiO_2 (750)	WO_x-TiO_2 (800)
$^{a}k_{app.}$ (min^{-1}) 10^{-2}	3.55	2.00	2.74	3.82	4.23	2.59	1.43
$^{b}k_{app.}$($g\ m^{-2}min^{-1}$)10^{-4}	5.19	1.44	2.70	4.85	6.28	4.96	4.05

$^{a}k_{app.}$ - Apparent first order constant
$^{b}k_{app.}$ - Apparent first order constant per unit of specific surface area

As the data show, the apparent first - order rate constants can be placed in the following order WO_x-TiO_2 (700)<WO_x-TiO_2 (650)<TiO_2 (500)<WO_x-TiO_2 (600)<WO_x-TiO_2(500)<WO_x-TiO_2 (800). The same order is obtained by dividing the apparent rate constant by specific surface area. These values point out the significance of exposure of active sites on their role in photocatalytic reaction. Although the specific surface area continuously drops with increasing calcination temperature, specific activity of the catalysts increases up to 700 °C as the result of complex structural changes. Thus, the synthesized WO_x-TiO_2 (700) powder can be used as a viable UV/visible-light driven photocatalyst for the degradation of azo-dye.

4. Conclusions

Nanocrystalline WO_x-TiO_2 powders were prepared by a sol-gel method combined with hydrothermal treatment. The XRD analysis revealed that WO_x-TiO_2 powders mostly consist of anatase phase with minor parts of rutile and tungsten oxides. The rise of calcination temperature caused an increase of crystallinity, crystallite and pore size, while specific surface area decreases continuously. All samples exhibited bimodal pore size distribution; smaller pores (3.7 nm) remain almost unchanged within the whole temperature range while larger mesopores were shifted towards large values, from 8.8 to 21 nm. Photocatalytic activity increases with calcination temperature up to 700 °C despite the lowering of the specific surface area, mainly due to increased pore size.

Acknowledgments

This work was supported by the Ministry of Education, Science and Technological Development of the Republic of Serbia (Projects number 172022, 172026, 172015, 172018, 172001 and III 45001).

5. References

1. G. Balasubramanian, D. Dionysiou, M. Suidan, I. Baudian, J. -M. Laîné, Evaluating the activities of immobilized TiO_2 powder films for the photocatalytic degradation of organic contaminants in water, Appl. Cat. B - Environ., 47 (2004) 73-84.
2. A. Turolla, A. Piazzoli, J. Farner Budarz, M. Wiesner, M. Antonelli, Experimental measurement and modelling of reactive species generation in TiO_2 nanoparticle photocatalysis, Chem. Eng. J., 271 (2015) 260-268.
3. S. Chin, E. Park, M. Kim, J. Jeong, G. -n. Bae, J. Jurng, Preparation of TiO_2 ultrafine nanopowder wit large surface area and its photocatalytic activity for gaseous nirtogen oxides, Powder Technol., 206 (2011) 306-311.

4. J. Dostanić, D. Lončarević, Lj. Rožić, S. Petrović, D. Mijin, D. M. Jovanović, Photocatalytic degradation of azo pyridone dye: Optimization using response surface methodology, Desalin. Water Treat., 51 (13-15) (2013) 2802-2812.
5. V. A. Sakkas, Md. A. Islam, C. Stalikas, T. A. Albanis, Photocatalytic degradation using design of experiments: A review and example of the Congo red degradation, J. Hazard Mater., 175 (2010) 33-44.
6. A. Fujishima, X. Zhang, D. A. Tryk, TiO_2 photocatalysis and related surface phenomena, Surf. Sci. Rep., 63 (2008) 515-582.
7. R. A. Carcel, L. Andronic, A. Duta, Photocatalytic activity and stability of TiO_2 and WO_3 thin films, Mater. Charact., 70 (2012) 68-73.
8. C. Anastasescu, N. Spataru, D. Culita, I. Atkinson, T. Spataru, V. Bratan, C. Munteanu, M. Anastasescu, C. Negrila, I. Balint, Chemically assembled light harvesting CuO_X-TiO_2 p-n heterostructures, Chem. Eng. J., 281 (2015) 303-311.
9. Y. Shen, A. C. Lua, Sol-gel synthesis of titanium oxide supported nickel catalysts for hydrogen and carbon production by methane decomposition, J. Power Sources, 280 (2015) 467-475.
10. W. Yajun, L. Kecheng, F. Changgen, Photocatalytic degradation of methyl orange by polyoxometalates supported on yttrium doped TiO_2, J. Rare Earth, 29(9) (2010) 866-875.
11. S. Stojadinović, N. Radić, R. Vasilić, M. Petković, P. Stefanović, Lj. Zeković, B. Grbić, Photocatalytic properties of TiO_2/WO_3 coatings formed by plasma electrolytic oxidation of titanium in 12-tungstosilicic acid, Appl. Cat. B-Environ., 126 (2012) 334-341.
12. S. Bai, H. Liu, J. Sun, Y. Tian, S. Chen, J. Song, R. Luo, D. Li, A. Chen, C. -C. Liu, Improvement of TiO_2 photocatalytic properties under visible light by WO_3/TiO_2 and MoO_3/TiO_2 composites, Appl. Surf. Sci., 338 (2015) 61.
13. S. A. K. Leghari, Sh. Sajjad, F. Chen, J. Zhang, WO_3/TiO_2 composite with morphology change via hydrothermal template-free route as an efficient visible light photocatalyst. Chem. Eng. J., 166 (2011) 906-915.
14. J. Caia, W. Xina, G. Liua, D. Lina, D. Zhua, Effect of calcination temperature on structural properties and photocatalytic activity of Mn-C-codoped TiO_2, Mater. Res., 19(2) (2016) 401- 407.
15. N. Labus, S. Mentus, Z. Z. Đurić, M. V. Nikolić, Influence of nitrogen and air atmosphere during thermal treatment on micro and nano sized powders and sintered TiO_2 specimens, Sci. Sinter., 46 (2014) 365-375.
16. M. A. Behnajady, H. Eskandarloo, N. Modirshahla, M. Shokri, Investigation of the effect of sol-gel synthesis variables on structural and photocatalytic properties of TiO_2 nanoparticles, Desalination, 278 (2011) 10-17.
17. A. Golubović, B. Simović, M. Šćepanović, D. Mijin, A. Matković, M. Grujić-Brojčin, B. Babić, Synthesis of anatase nano powders by sol-gel method and influence of temperatures of calcinations to their photocatalitic properties, Sci. Sinter., 47 (2015) 41-49.
18. I. Jouanny, S. Labdi, P. Aubert, C. Buscema, O. Maciejak, M. H. Berger, Structural and mechanical properties of titanium oxide thin films for biomedical application, Thin Solid Film, 518(12) (2010) 3212-3217.
19. P. Huang, F. Wang, K. Xu, Y. Han., Mechanical properties of titania prepared by plasma electolytic oxidation at different voltages, Surf. Coat. Tech., 201 (2007) 5168-5171.
20. Y. Gaillard, E. Jimenez-Pique, A.R. Gonzalez-Elipe, Nanoindentation of TiO_2 thin films with different microstructures, J. Phys. D Appl. Phys., 42 (2009) 145305.
21. L. Borgese, E. Bontempi, M. Gelfi, L.E. Depero, P. Goudeau, G. Geandier, I. D. Thiaudiére, Microstructure and elastic properties of atomic layer deposited TiO_2 anatase thin films, Acta Mater., 59 (2011) 2891-2900.

22. V. D. Mote, Y. Purushotham, B. Dole, Williamson-Hall analysis in estimation of lattice strain in nanometer-sized ZnO particles. J. Theor. Appl. Phys., 6:6 (2012).
23. H. P. Klug, L. E. Alexander, X-ray Diffraction Procedure for Polycrystaline and Amorphous Materials, 2nd ed., Wiley, New York 1974.
24. K. Sing, D. Everet, R. Haul, L. Moscou, R. Pierotti, J. Rouquerol, T. Siemieniewska, Reporting Physisorption data for gas/solid systems with Special Reference to the Determination of Surface Area and Porosity, Pure Appl. Chem., 57 (1985) 603-619.
25. E. P. Barrett, L. G. Joyner, P. H. Halenda, The Determination of Pore Volume and Area Distributions in Porous Substances. I. Computations from Nitrogen Isotherms, J. Am. Chem. Soc., 73 (1951) 373-380.
26. C. R. Tubio, F. Guitián, J. R. Salgueiro, A. Gil, Anatase and rutile TiO_2 monodisperse by rapid thermal annealing: A method to avoid sintering at high temperatures, Mater. Lett., 141 (2015) 203-206.
27. T. B. Grosh, S. Dhabal, A. K. Datta, On crystallite size dependence of phase stability of nanocrystalline TiO_2, J. Appl. Phys., 94 (7) (2003) 4577-4582.
28. S. Bakardjieva, J. Šubrt, V. Štengla, M. J. Dianez, M. J. Sayagues, Photoactivity of anatase-rutile TiO_2 nanocrystalline mixtures obtained by heat treatment of homogeneously precipitated anatase, Appl. Catal. B- Environ., 58 (2005) 193-202.
29. M. Rani, S. J. Abbas, S. K. Tripathi, Influence of annealing temperature and organic dyes as sensitizers on sol-gel derived TiO_2 films, Mat. Sci. Eng. C-Bio S, 187 (2014) 75 -82.
30. V. Likodimosa, A. Chrysia, M. Calamiotoua, C. Fernández-Rodriguez, J.M. Doña Rodriguez, D. D. Dionysiou, P. Falaras, Microstructure and charge trapping assesment in highly reactive mixed phase TiO_2 photocatalysts, Appl. Catal. B-Environ., 192 (2016) 242-252.
31. Z. Chen, D. D. Dionysiou, A comparative study on physicochemical properties and photocatalytic behavior of macroporous TiO_2-P25 composite films and macroporous TiO_2 films coated on stainless steel substrate, Appl. Catal. A-Gen., 317 (2007) 129-137.

Садржај: *У овом раду је за синтезу WO_x-TiO_2 прахова коришћена сол-гел метода у комбинацији са хидротермалним поступком. Утицај температуре синтеровања на структуру и текстурална својства је испитиван применом методе дифракције X-зрака и анализом адсорпционо-десорпционих изотерми азота. Величина кристалита, параметри кристалне решетке и њено напрезање је одређивано помоћу Williamson-Hall методе. Резултати су показали да са порастом температуре синтеровања долази до раста односа c/a параметара јединичне ћелије изазване истезањем у правцу c-осе. Адсорпционо-десорпциона анализа је показала да сви узорци поседују бимодалну расподелу пора у области мезопора. Са порастом температуре синтеровања установљено је да долази до померања преовлађујућег пречника пора ка већим вредностима. Запажен је пораст каталитичке активности код узорака жарених до 700 °C, док даљи пораст температуре синтеровања изазива значајан пад активности.*
Кључне речи: *WO_x-TiO_2 прах; синтеровање; мезопорозна структура; фотокаталитичка деградација; азо боја*